

Analysis of Hydrogen Enriched Flames by Laser Diagnostics

Andrea Olivani, Fabio Cozzi, Aldo Coghe

Dipartimento di Energetica, Politecnico di Milano, Milan, Italy
andrea.olivani@polimi.it, fabio.cozzi@polimi.it, aldo.coghe@polimi.it

Abstract The flame structure and flow field modifications induced in a confined lean non-premixed natural gas swirled flame by hydrogen addition were experimentally investigated using non-intrusive laser based diagnostic techniques: PIV and LDV were used for a comprehensive analysis of the velocity field and the Rayleigh scattering technique for the local temperature distribution. Measurements were performed on a straight exit laboratory burner with no quarl cone; the flame was stabilized at the end of two concentric pipes with the annulus supplying swirled air and the central pipe delivering the fuel. In order to improve the mixing between reactants, the fuel mixture was injected transversally toward the swirling air flow. Experiments were carried out at varying hydrogen content in the range 0% - 100% of the total volumetric fuel flow rate.

The analysis of vorticity maps and velocity PDFs underlined that in the region located between the Central Toroidal Recirculation Zone (CTRZ) and the Corner Recirculation Zone (CRZ) took place an intense mixing process between reactants coming from the burner outlet and hot products from recirculation zones. Also temperature PDFs analysis revealed bimodal distributions in the same regions. Considering each bimodal distribution as the overlap of two distinct Gaussian distributions, it was possible to evaluate the temperature of each stream in the mixing layer and to characterized the mixing process.

1 Introduction

In the last decades the scientific community has shown an increasing interest in the hydrogen field. This renewed interest on hydrogen as an energy carrier is mainly due to the global climate change and to the expected depletion of conventional hydrocarbon fuels. Moreover, hydrogen as a substitute for fossil fuels is attractive since it has the potentialities to drastically alleviating the emissions problems, with the exception of NO_x compounds. Changing from hydrocarbon to alternative fuels is expected to be a very complex, enormously expensive and time-consuming process even if all the necessary technologies would be already available, which is not the case. The present work is focalized on the use of hydrogen in traditional combustion systems and in particular in a non-premixed swirl stabilized burner.

Swirling motion is regarded as an efficient way to improve and control the mixing rate between fuel and oxidant streams and to improve flame stabilization through the swirl-induced recirculation of hot products. The basic principle is that above a critical swirl level ($S > 0.6$), an expansion of the swirling flow leads to vortex breakdown with the accompanying flow reversal in the core region, the so called CTRZ. In swirl stabilized flames, the combustion process is strongly influenced by the dimension and shape of the CTRZ, because the reverse flow carries hot combustion products and radicals backwards and supplies energy for the ignition of the incoming fuel-air stream. Swirling flames have been studied extensively for many years; however, most of these studies are focused on premixed flames and only relatively few works are available on non-premixed swirl flames. The most recent experimental investigations take advantage of non-intrusive laser based diagnostic techniques to better understand the chemistry and fluid dynamics of reacting swirling flows.

Schefer (2003) and Schefer et al. (2002) conducted experiments in an enclosed swirl-stabilized combustor representing geometric features of advanced gas turbines and evidenced that

the flame structure was influenced by the fuel composition. They found that addition of H₂ to CH₄ in premixed flames extended the flame stability and lean blowout limit. This was due to the fact that, as evidenced by OH planar laser-induced fluorescence (PLIF) images, the reaction zone became broader and more intense when H₂ was added to CH₄. Moreover, for a given chemical energy input, the hydrogen enriched flame was shorter and more intense. Pollutant emissions measurements showed that a significant reduction of CO was achieved by the addition of hydrogen to the fuel due to the above mentioned higher radical concentration. Ji and Gore (2002) employed particle image velocimetry to obtain instantaneous and time-averaged flow fields in an unconfined swirl-stabilized burner, with and without combustion. Many smaller-scale vortices were observed in the instantaneous flow fields in contrast to the averaged field with a single large vortex and the vorticity magnitude in the flame was significantly higher than that in the isothermal condition. Based on the differences in the mean and instantaneous flow structures, they proposed that the latter should be used to evaluate transient combustion phenomena.

Only few experimental works are focused on temperature measurements inside swirl flames. Qi et al. (1997) presented an experimental study on the effect of swirl in premixed flames based upon thermocouple temperature measurements. The PDF of temperature data revealed a bimodal distribution in the shear layer region of the flame having two distinct well defined temperature peaks, corresponding to the unburned and recirculating gas. Moreover, the mean and fluctuating temperature measurements provided insight into the local thermal turbulent structure of premixed swirl flames. Temperature measurements using the non-intrusive Rayleigh scattering technique were performed by Tangirala and Driscoll (1988) in non-premixed CH₄/H₂/Air swirl flames. They quantified the level of unmixedness, as characterized by temperature fluctuations, in the limit of very high swirl ($S = 2.6$) and evidenced that even at high swirl the non-premixed flame didn't become "well-stirred". Indeed the measured temperature fluctuations remained significantly larger than those observed in swirl premixed flames by Halthore and Gouldin (1986). Also in two recent experimental investigations by Weigand et al. (2006) and Meier et al. (2006), on swirling CH₄/air non-premixed flames, temperature fluctuations, measured with the Raman scattering technique, reached a level of 500-600 K close to the fuel nozzle and decreased to 40-70 K at larger heights. These high temperature fluctuations close to the nozzle, together with single-shot images of OH and CH, evidenced that the CTRZ is not a stationary vortex stable in time and space, but rather is subjected to significant fluctuations.

In the present work the combustion characteristics of natural gas-hydrogen-air reacting mixtures were investigated inside a model swirl combustor; the use of a model combustor was suitable for the application of various non-intrusive laser based diagnostic techniques for both the thermal and the fluid-dynamic analysis. LDV and PIV techniques were extensively used to characterize the flow field and to gain detailed experimental information of the near burner throat aerodynamics, and the Rayleigh scattering technique was applied for temperature measurements and to study the mixing process between reactants and combustion products.

2 Experimental Set-Up and Operative Conditions

The swirl burner, operating at ambient pressure, had no quarl cone and it was fired vertically upwards with the flame stabilized at the end of two concentric pipes with the annulus supplying swirled air and the central pipe delivering the fuel mixture. The inner and outer radius of the air annulus were respectively $R_i = 7.5$ mm and $R_b = 18$ mm. Air swirl motion was imparted through axial plus tangential air entries and variation of the relative amounts of axial and tangential airflows controlled the swirl strength. In order to improve reactants mixing, the fuel mixture was injected transversally toward the swirling air flow through 8 holes ($d = 3$ mm) symmetrically distributed on the periphery of the fuel pipe. The holes were located 3 mm upstream from the exit throat of the

burner. The combustion zone was enclosed by a water cooled stainless steel chamber (internal diameter = 194 mm; height = 290 mm). The ratio of chamber diameter to burner diameter was 5 to 1. The combustion chamber was alternatively equipped with quartz windows for flame visualization and measurements by optical techniques or with slotted metal sheets for introducing probes. A conical natural draught hood, with a 4:1 area contraction, provided the exhaust of the burned gases.

In order to investigate the effects of hydrogen addition to natural gas, the air flow field was kept constant, for all experimental conditions, by maintaining fixed both the swirl number ($S = 0.82$) and the air Reynolds number ($Re_{air} = 20150$) at the burner exit. The swirl number (S) was evaluated using axial and tangential velocity profiles measured by LDV at 1 mm downstream from the exit plane of the burner, under isothermal conditions, following the definition of Gupta et al. (1984) and neglecting the turbulent stress and the pressure terms.

By keeping constant the volumetric fuel mixture flow rate, at 32 NI/min, the hydrogen content in the fuel mixture was varied between 0% and 100% of the total volumetric fuel flow; correspondingly the input thermal power decreased from 20.1 kW (0% H_2) to 5.8 kW (100% H_2), and the global equivalence ratio was reduced from 0.71 (0% H_2) to 0.17 (100% H_2). The fuel jet Reynolds number (Re_{fuel}), associated to the hole diameter, was estimated at ambient temperature by using the dynamic viscosity calculated from a polynomial fit of the experimental data (@ ~ 300 K) of Nabizadeh and Mayinger (1999). All data regarding the experimental conditions are summarized in Table 1. More details on the experimental set-up and burner operating conditions can be found in the works of Coghe et al. (2004) and Cozzi and Coghe (2006).

Table 1 Burner operating conditions at fixed fuel flow rate

$\%H_2$	\dot{m}_{fuel} [g/s]	\dot{m}_{air} [g/s]	Re_{fuel}	Φ_{global}	P_{input} [kW]
0	0.425	9.478	2179	0.71	20.1
80	0.123	9.478	749	0.28	8.6
100	0.048	9.478	302	0.17	5.8

2.1 Flow Field Measuring Techniques

Time resolved point velocity measurements were performed using a two-component fiber optics Laser Doppler Velocimeter (LDV) equipped with an Argon ion laser and a Bragg cell (40 MHz) frequency shift for directional ambiguity resolution. The LDV was operated in the backscatter mode and the signal processors were two Burst Spectrum Analysers (BSA – Dantec). Alumina particles (nominal diameter 2 μm) were used to determine gas velocity distribution. The relatively high density of the alumina particles and their size limits their capability to follow high frequency flow fluctuations, but allowed correct definition of the mean flow field.

At least 3000 instantaneous velocity data were used for statistical analysis, with estimated statistical errors of less than 4% in the mean values and 6% in the RMS fluctuations. Moreover, the transit time of the individual particle through the measuring volume is used as weighting factor to compensate for the effect of velocity bias.

PIV measurements were obtained with a double pulsed Nd-YAG laser, operating at 532 nm. The seeding methodology was the same used for the LDV measurements. Images of Mie-scattered light from the seed particles were recorded utilizing a digital camera. The camera (Dantec HiSense PIV/PLIF Camera) had a 1280 by 1024 pixel image and was placed normal to the laser sheet. A Micro-Nikkor (f = 60 mm) objective was used to collect the scattered light, and the resulting field of view was approximately 100 (horizontal) by 80 (vertical) mm^2 . Background light and flame luminescence were removed using a 10-nm band-pass filter centered at 532 nm. The two images

were recorded on sequential frames to allow a cross-correlation analysis of the data. In this study, at least 200 images were taken for each experimental condition to ensure accurate data analysis. Considering an interrogation area of 32 by 32 pxl, with a 50% overlap, the spatial resolution in velocity measurements was about 1.2 by 1.2 mm². Considering that U and V are respectively the axial and radial velocity components, the vorticity is calculated from the 2-D velocity maps as,

$$\omega = \frac{\partial U}{\partial r} - \frac{\partial V}{\partial z} \quad (1)$$

2.2 Rayleigh Scattering Technique

As reported by Kruppa and Strube (1994), Rayleigh scattering intensity is given by the following formula,

$$I = C(\partial\sigma/\partial\Omega)\Omega L N I_0 \quad (2)$$

where C is the detection efficiency, $(\partial\sigma/\partial\Omega)$ is the effective differential scattering cross section, Ω is the solid angle of collection, L is the length of the probe volume, N is the number density of molecules, I_0 is the intensity of the incident laser light. In experiments where the scattering cross section can be regarded as a known constant, the Rayleigh intensity is directly proportional to the total number density. Then, the equation of the ideal gas permits to calculate the temperature as,

$$I = C(\partial\sigma/\partial\Omega)\Omega L \frac{pA_0}{RT} I_0 = \frac{K}{T}(\partial\sigma/\partial\Omega) \quad (3)$$

where A_0 is Avogadro's number, R is the universal gas constant and K is a constant which depends on the experimental conditions and can be evaluated by calibration in non-reacting flows. As evidenced from Eq. 3, the Rayleigh scattering intensity is inversely proportional to the temperature of the gas. In the present work, the Rayleigh cross section of natural gas was calculated from the fuel composition and from the cross sections of major chemical species inside the mixture. Values of cross sections were taken from Namer and Schefer (1985).

2.2.1 Rayleigh Scattering Experimental Apparatus

The laser system used in this experimental activity was a pulsed Nd:YAG laser, operating at 532 nm. The pulse energy was kept close to 200 mJ/pulse with a pulse duration of less than 10 ns and a repetition rate of 8 Hz. The Rayleigh scattered light was collected at the right angle of the incident beam by a 300 mm focal length lens ($d = 50$ mm), at unit magnification, on the 1 mm slit of a monochromator (Jobin Yvon, model H20UV; aperture f/4.2; 0.5 nm resolution). The dimensions of the cylindrical scattering volume, as determined by the laser beam and collection optics, were approximately 1 mm in height and 50 μ m in diameter. Scattered photons were detected by a photomultiplier tube (PMT) positioned on the monochromator exit. The PMT output was recorded using a Gated Integrator/Boxcar Averager (SR250, Stanford Research System). All Rayleigh scattering measurements reported are shot-by-shot measurements. The output from the boxcar was digitized by a 16-bit ADC board and acquired by a PC for data recording and analysis.

2.2.2 Rayleigh Signals Analysis and Data Treatment

In order to obtain quantitative temperature measurements, the acquired Rayleigh scattering intensities were corrected for background level, due to laser light scattered by the surroundings

(mirrors, lenses, etc.). The background level was estimated by injecting helium into the laser probe volume and by acquiring the output signal of the photomultiplier tube. Since the Rayleigh cross section of helium is two orders of magnitude smaller than the other gases, it was assumed that the recorded signal was mainly due to the background level and not to the Rayleigh scattering of helium. Regarding the spontaneous luminosity of the flame, due to the very short time interval for acquisition of the gated boxcar integrator (20 ns), the background flame luminescence, recorded with the laser off, was found to be negligible.

The calibration constant K in Eq. 3 was determined at room temperature by recording the Rayleigh scattering intensity with air flowing inside the probe volume. The calibration was performed both before and after measurements inside the flame, and if the two values were different from each other more than 2 percent, data were rejected. This was necessary in order to guarantee that the intensity of the incident laser beam was not significantly changing during measurements.

In order to compensate for effects of spatial non-uniformities of the collection system, the background level (estimated using helium) and the calibration constant K (estimated using air at ambient temperature) were evaluated for all the different measuring positions.

For each measuring position, 1000 single shot data were acquired with a PC for storage and analysis. For each position, the mean value of the Rayleigh scattering intensity (I_i), together with the standard deviation and the probability density function (PDF), were calculated. Finally, temperature values were calculated using Eq. 4:

$$T_{flame} = T_{air} \frac{(I_{air} - I_{He})}{(\partial\sigma/\partial\Omega)_{air}} \frac{(\partial\sigma/\partial\Omega)_{flame}}{(I_{flame} - I_{He})} \quad (4)$$

2.2.3 Considerations on Rayleigh Cross Section

As evidenced in Eq. 2, the Rayleigh scattered intensity depends on both the total number density and the gas composition. By judicious tailoring of fuel and oxidizer flows, the Rayleigh cross section variation with combustion can be held to few percent. In these instances changes in the Rayleigh intensity track directly with the temperature (at constant pressure).

Considering the full conversion of fuels (natural gas and hydrogen) into carbon dioxide and water it was possible to estimate the Rayleigh cross section of reactants and products for desired reacting mixtures. In Fig. 1 the values of the cross sections of reactants and products for different hydrogen contents, at fixed volumetric fuel flow rate, are shown; these values are also compared with the cross section of air. The differences between $(\partial\sigma/\partial\Omega)_{reactants}$ vs. $(\partial\sigma/\partial\Omega)_{products}$ and $(\partial\sigma/\partial\Omega)_{products}$ vs. $(\partial\sigma/\partial\Omega)_{air}$ are generally small, and in most cases smaller than 5 %.

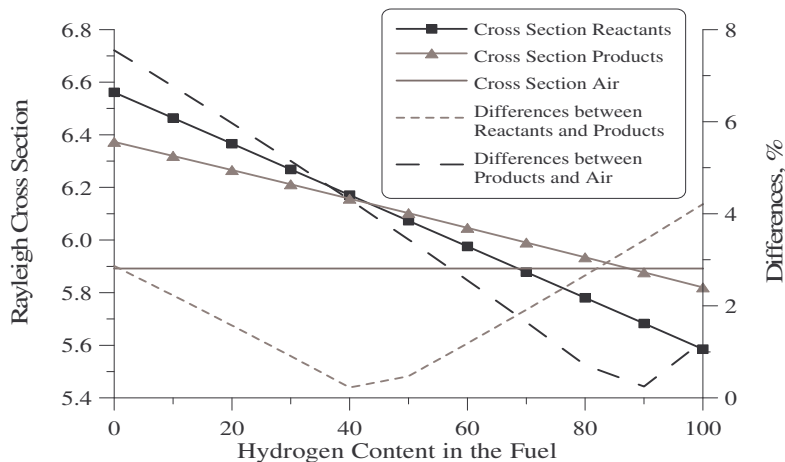


Fig. 1 Variations of the Rayleigh cross section for various hydrogen content

In a non-premixed flame, the local equivalence ratio can be quite different from the global condition of the system. It is then useful, for a fixed fuel composition (i.e. for a fixed mixture of NG and H₂), to analyze the variations of reactants and products cross sections with changing equivalence ratio. The results of this study are summarized in Fig. 2. Since global equivalence ratios that are used in the present work correspond to lean conditions, the local equivalence ratio is varied between 0.1 and 1 and a dashed line is used to indicate the global equivalence ratio of the mixtures used during the experimental investigation. As can be observed, differences between $(\partial\sigma/\partial\Omega)_{reactants}$ and $(\partial\sigma/\partial\Omega)_{products}$ as well as differences between $(\partial\sigma/\partial\Omega)_{products}$ and $(\partial\sigma/\partial\Omega)_{air}$ are generally small.

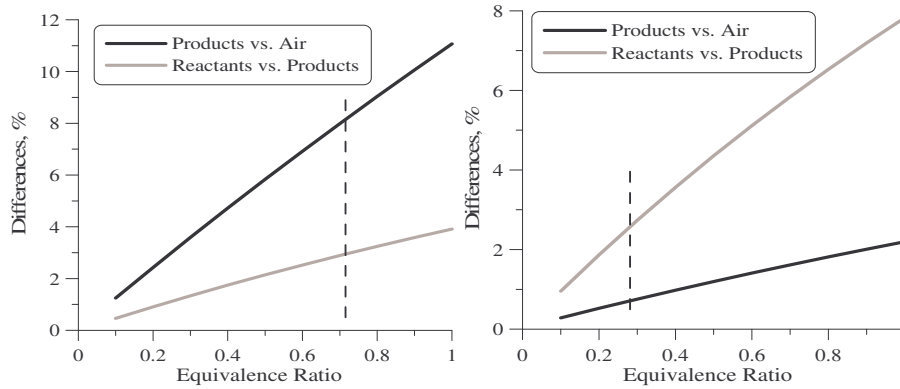


Fig. 2 Variation of the Rayleigh cross section with the equivalence ratio for a fixed fuel composition: 0% H₂ (left); 80% H₂ (right)

In using a NG-H₂ fuel mixture a potential problem could arise. If the mixing is governed entirely by molecular properties, the differing molecular diffusivities of hydrogen and hydrocarbons could complicate the diffusion flame structure. Drake et al. (1986) showed that differential diffusion is negligible in jet flames for Reynolds numbers greater than 8500. Tangirala and Driscoll (1988) performed Rayleigh scattering measurements on a swirl flow, under non-reacting conditions, with a H₂-CH₄-air mixture. In their experiment the fuel composition was selected in order to obtain a Rayleigh cross section of the fuel mixture equal to that of air. Rayleigh intensity measurements in various spatial locations inside the flow field evidenced intensity fluctuation below 4%, and thus they concluded that differential diffusion effect was negligible. In the present case, the Reynolds number of the swirling air is fixed at 20150 for all flames, which is well above the limit indicated by Drake et al. (1986) and thus it is assumed that the mixing is entirely governed by turbulence.

All these considerations and calculations on Rayleigh cross sections of reactants and products, for different fuel compositions and at different global and local equivalence ratios, lead to the conclusion that, in these cases, errors related to uncertainties in the chemical composition of the mixture were within acceptable bounds. Moreover, these uncertainties were included in the global error analysis reported in the next paragraph.

2.2.4 Errors Analysis

Statistical errors on the measured Rayleigh scattering intensity was estimated as,

$$\varepsilon_{I_i} = t_{95\%} \frac{\sigma_{I_i}}{\sqrt{N}} \quad (5)$$

where ε_{I_i} is the uncertainty on the acquired scattering signals I_{air} , I_{flame} and I_{He} ; σ_{I_i} are the corresponding standard deviations; N is the number of measurements; $t_{95\%}$ is the estimator for the Student distribution at 95% probability. Then, recalling Eq. 3 and considering that temperature measurements were also affected by uncertainties on the chemical composition of the mixture inside the probe volume, the total error was estimated as,

$$\varepsilon_{TOT} = \sqrt{\left(\frac{\partial T_{flame}}{\partial \left[(\partial \sigma / \partial \Omega)_{flame} \right]} \varepsilon_{CS} \right)^2 + \sum_i \left(\frac{\partial T_{flame}}{\partial I_i} \varepsilon_{I_i} \right)^2} \quad (6)$$

where ε_{CS} is the uncertainty on cross section evaluated by the considerations reported in the previous paragraph. Recalling data reported in Fig. 2, it was assumed that $\varepsilon_{CS} \approx 5\%$ outside the reaction zone and $\varepsilon_{CS} \approx 15\%$ inside the reaction zone where the local equivalence ratio is close to unity; thus $\varepsilon_{TOT} \approx 65 K$ outside the reaction zone and $\varepsilon_{TOT} \approx 110 K$ inside the reaction zone.

3 Results and Discussion

3.1 Flow Field Measurements

Streamlines superimposed to flame pictures, in a region located immediately downstream of the burner exit, are reported in Fig. 3. In all maps, the reactants outlet is located in the bottom center of the velocity field, between radial coordinates of -18 mm and 18 mm. The combustor wall is outside the field of view. Fig. 3 clearly indicates the existence of a central toroidal recirculation zone (CTRZ) and a corner recirculation zone (CRZ). The CTRZ is the broad region of reverse flow confined by the expanding air stream and extending back toward the burner head. The CRZ, which is partially outside the PIV field of view, is produced by the confinement due to the chamber wall and the bottom plane and it extends externally to the air stream.

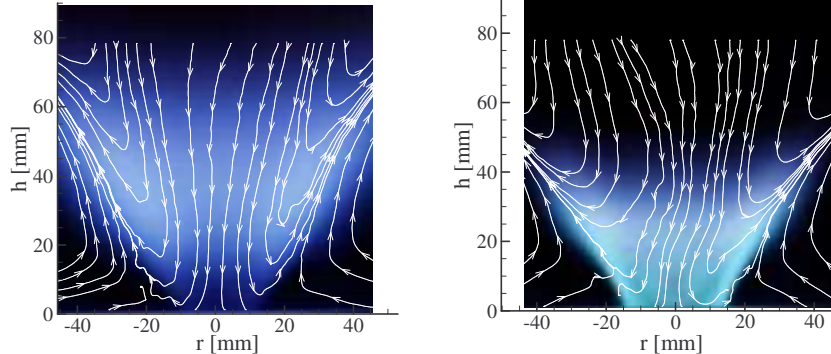


Fig. 3 Superimposition of streamlines and pictures: 0% hydrogen (left); 80% hydrogen (right)

The superimposition of streamlines and flame pictures, clearly shows that one of the effects of hydrogen addition is to move the heat release region much closer to the reactant outlet. Indeed, when the hydrogen content in the fuel mixture increases, the luminous part of the flame becomes brighter, moves toward the burner head and partially penetrates in the air annulus, indicating that the overall reaction rate is increasing. Indeed, as observed by Jackson et al. (2003), hydrogen oxidation supplies energy and radical pool to sustain and enhance the natural gas oxidation allowing NG ignition under conditions at which otherwise it might not be possible to sustain a stable flame. As the hydrogen percentage in the fuel mixture increases, the imaging of the unfiltered spontaneous flame emission show a monotonic decrease in the visible flame size. However, this reduction seems to be mainly due to the decrease of both the global equivalence ratio and the input thermal power with increasing hydrogen content keeping constant the total volumetric fuel flow rate (Table 1).

Thus hydrogen addition affects the flow field by changing both the location and rates of heat release and, as a consequence, the higher thermal expansion of hot combustion products pushes the swirling air stream outwards in the radial direction, as clearly shown by streamlines position. Indeed

the radial extension of the CTRZ is smaller for the 0% hydrogen flame compared to the 80% hydrogen one.

Fig. 4 show the vorticity fields calculated from the average velocity fields for the 0% and the 80% hydrogen flames. Regions of positive vorticity are associated with counterclockwise rotating flows, while regions of negative vorticity are associated with clockwise rotating flows. In order to better understand where the high vorticity regions are located in the flow field, streamlines are added on vorticity maps. For all cases, peak vorticity magnitudes of about 3000 s^{-1} are observed in the shear layers between the CTRZ and the CRZ. This result underlines that in this region takes place an intense mixing process between reactants coming from the burner head and hot products from recirculation zones and so it is mainly in this region of the flow field that hot combustion products and radicals provide energy for the ignition of the incoming fuel-air stream. Moreover, PIV measurements evidence that the displacement of the reaction zone, due to hydrogen addition, affects not only the velocity fields, but also the regions of high vorticity levels, leading to a decrease in their size with increasing hydrogen content.

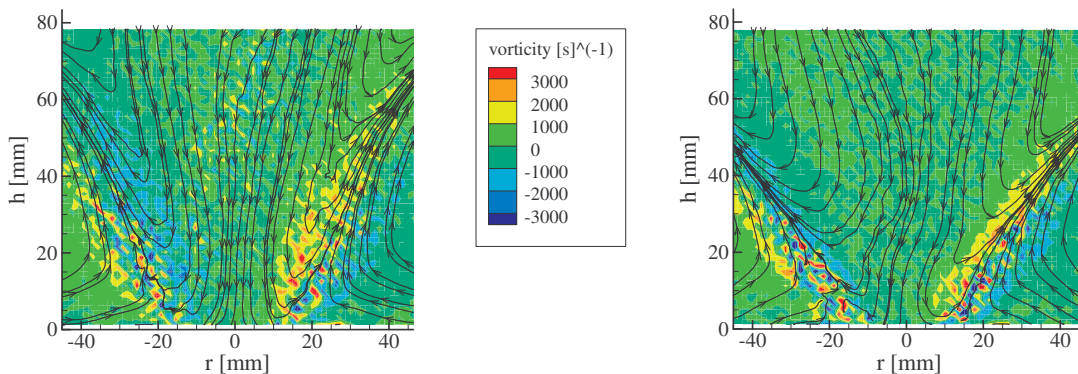


Fig. 4 Superimposition of the vorticity field and streamlines: 0% hydrogen (left); 80% hydrogen (right)

The probability density functions (PDF) of LDV data allow to investigate how the different structures of a swirl flow interact with each other in the shear layer between the CTRZ and the CRZ. The PDF analysis is carried out for all velocity components along a radius at $h/R_b = 0.56$ above the burner head for various fuel mixtures and results are summarized in Fig. 5 for the axial and the radial velocity components for the 80% hydrogen flame.

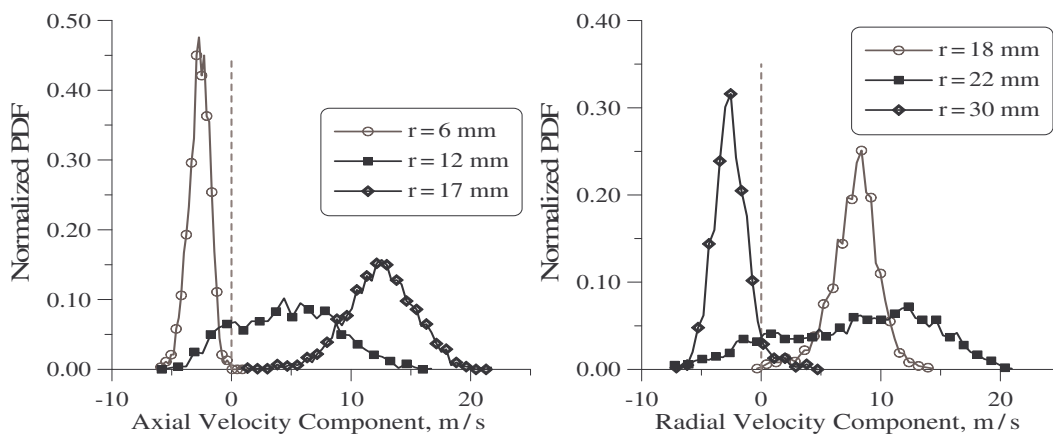


Fig. 5 80% H_2 flame: evolution of the axial (left) and radial (right) velocity PDFs along a radial traverse at $h/R_b = 0.56$

Generally, axial velocity PDFs are clearly Gaussian fully inside the CTRZ and the CRZ, while they become more flat in the shear layer region, where there is a mixing between the out flowing reactants stream and the reversed flow. Likewise, radial velocity PDFs are characterized by negative and positive velocity values in the mixing layer between the out flowing reactants stream and the CRZ. Vorticity maps (Fig. 4) evidence the existence of two shear layers laying close

together: the first one located between the CTRZ and the out-flowing reactants stream, and the second one generated by the interaction between the out-flowing reactants stream and the CRZ. Considering the right part (i.e. $0 \text{ mm} < r < 45 \text{ mm}$) of vorticity maps and moving along a radius, at $h/R_b = 0.56$ ($h = 10 \text{ mm}$), from the center of the combustion chamber, the two shear layers described above are found: first a zone of counterclockwise rotating vortices, around $0.56 < r/R_b < 1.1$ ($10 \text{ mm} < r < 20 \text{ mm}$), and after an area of clockwise rotating ones, around $0.8 < r/R_b < 1.5$ ($15 \text{ mm} < r < 27 \text{ mm}$). As previously observed, due to unsteadiness of the flow field, the two regions partially overlap with each other. As reported in Fig. 5 (left), intermittency of the axial velocity component is mainly observed at $r \approx 10\text{-}15 \text{ mm}$, and thus counterclockwise rotating vortices are associated with the interaction between the downward reverse flow and the upward stream from the burner head. In a similar manner, intermittency of the radial velocity component, observed at $r \approx 17\text{-}30 \text{ mm}$ (Fig. 5 right), is associated with clockwise rotating vortices, generated by the mixing between the out-flowing reactants stream (going outward) and the flow coming from the CRZ (going inward).

3.3 Temperature Measurements

Fig. 6 illustrates the effects of H_2 addition to natural gas on temperature profiles. Inside the reaction zone region (i.e. $0.5 < r/R_b < 0.9$), as hydrogen is added to the fuel mixture, due to faster heat release, the temperature greatly increases. For all curves the region corresponding to the out-flowing air stream is clearly visible with low temperature levels. At the periphery (i.e. $r/R_b > 1.7$), a region characterized by quite uniform temperature values is established and this is related with the formation of the CRZ. Moreover, as the hydrogen content increases, the average gas temperature in the CRZ decreases, due to both a decrease of the global equivalence ratio and of the input thermal power (Table 1). For the same reasons also temperature values in out-flowing stream region and in the central part of the combustion chamber decrease with increasing hydrogen content.

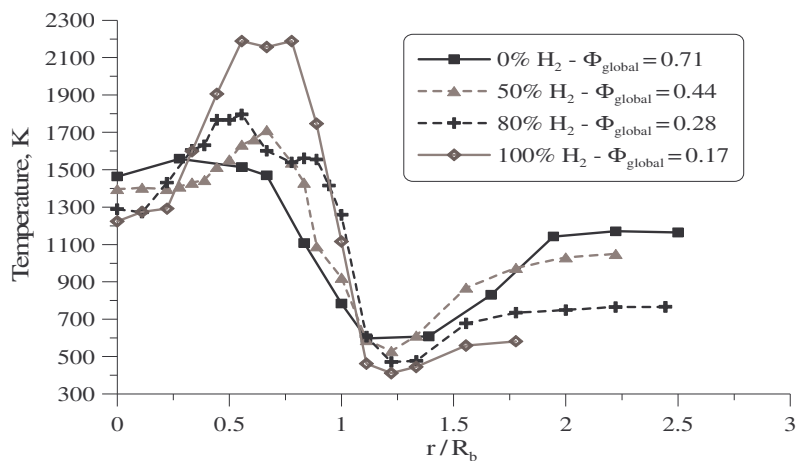


Fig. 6 Temperature radial profiles at $h/R_b = 0.56$ ($h = 10 \text{ mm}$) above the reactants outlet

The peak temperature of the 100% H_2 flame (2200 K) is quite close to its adiabatic equilibrium value estimated for unit equivalence ratio (2383 K), while the peak temperature of the 80% H_2 flames reduces to about 1800 K, which is significantly below the stoichiometric value of 2307 K. The peak temperature for the NG flame (1550 K) is even much lower than the adiabatic stoichiometric temperature of 2226 K. Differences between peak temperatures and adiabatic flame temperatures are mainly due to radiative heat losses. In the present work no visible continuous soot emission is detected for $\text{NG}+\text{H}_2$ flames. However, broadband radiation from CO_2 and bands radiation from H_2O molecules is still present and contributes to lower the actual temperature values

as compared to the adiabatic ones. Poor agreements with equilibrium temperatures were found in NG+H₂ jet diffusion flames by Choudhuri and Gollahalli (2003).

As evidenced by LDV and PIV measurements, the region located between the outer boundary of the CTRZ and the inner boundary of the CRZ is characterized by an intense mixing process between three different flows; also the analysis of Rayleigh scattering intensity PDF reveals bimodality in this region. Following Vanoverberghe et al. (2004), the measured intensity PDF is approximated by a curve fit (\widetilde{pdf}) which is the sum of two Gaussian distributions g_1 and g_2 :

$$\widetilde{pdf} = s \cdot g_1 + (1-s) \cdot g_2 \quad \text{where} \quad g_i = \frac{1}{\sigma_i (2\pi)^{1/2}} \exp \left[-\frac{(x-\mu_i)^2}{2\sigma_i^2} \right] \quad (7)$$

μ_1 and μ_2 are the mean values of the Rayleigh scattering intensity which are used to calculate separately the mean temperatures of the two mixing flows using Eq. 4. The share parameter (s) can be interpreted as the probability that the probe volume is located inside one of the two streams with different mean temperature and changes between 0 and 1. For all bimodal distributions, μ_i , σ_i and s are evaluated from an interpolation of experimental PDFs in the least-squares sense. In Fig. 7 the spatial evolution of PDFs of Rayleigh scattering intensities for the 80% H₂ flame are reported for different radial positions in the range $0.94 < r/R_b < 1.2$ (17 – 22 mm). As can be easily observed, with increasing distance from the center of the flame, the absolute mean value of the Rayleigh scattering intensity increases, corresponding to a decrease in the mean temperature of the gases. Moreover, the bimodal characteristic of Rayleigh intensity PDFs is clearly visible, showing the mixing of the two flows at different temperatures: hot combustion products from the reaction zone and cold fuel-air mixture from the burner head.

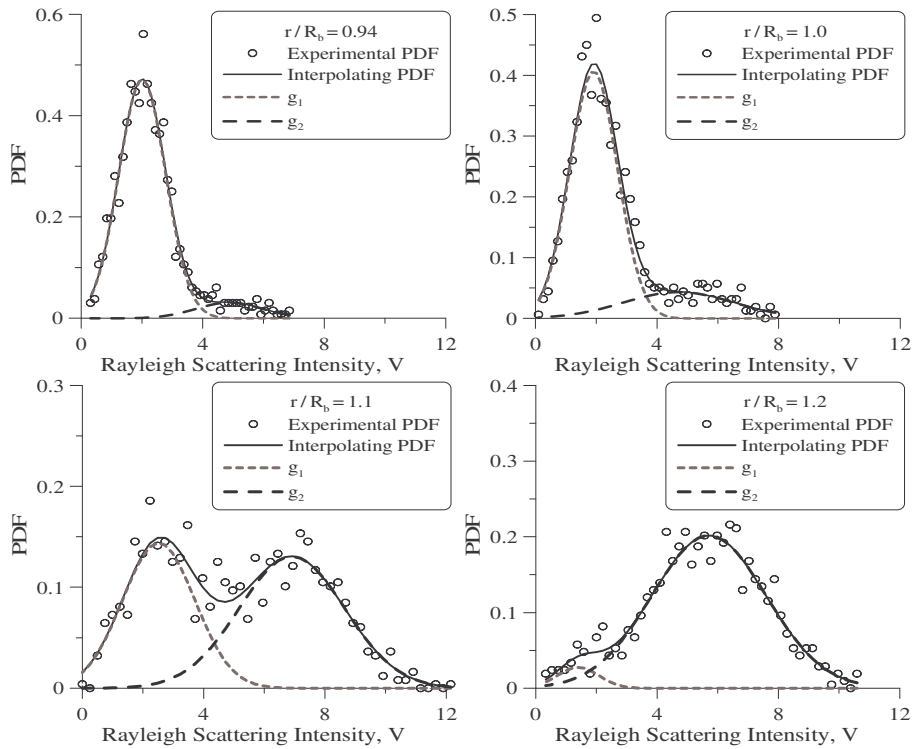


Fig. 7 Spatial evolution of PDFs of Rayleigh scattering intensities for the 80% H₂ flame in the range $0.94 < r/R_b < 1.2$

Radial profiles of the mean temperature are reported together with temperatures of the mixing flows in Fig. 8 and Fig. 9. In both cases the region corresponding to the mixing layer between the outflowing gas stream and the flame zone, $0.8 < r/R_b < 1.2$ (14 mm < r < 22 mm), is characterized

by bimodal temperature distributions. It is also interesting to note that temperatures of the “hot stream” are generally much higher than the maximum value of the mean temperature profile. Hence, even if the global flow field is characterized by an intense mixing process, generated by the swirl motion, local temperature non-uniformities are still present and may have a considerable impact on flame stability and pollutants emissions, as evidenced by Olivani et al. (2005). Moreover, with increasing hydrogen content inside the fuel mixture, a second region characterized by bimodal temperature PDFs appears in the central part of the combustion chamber. The values of the temperature of the two mixing streams suggest that they correspond to recirculating combustion products ($T \approx 900$ K) and hot gases inside the reaction zone ($T > 2000$ K).

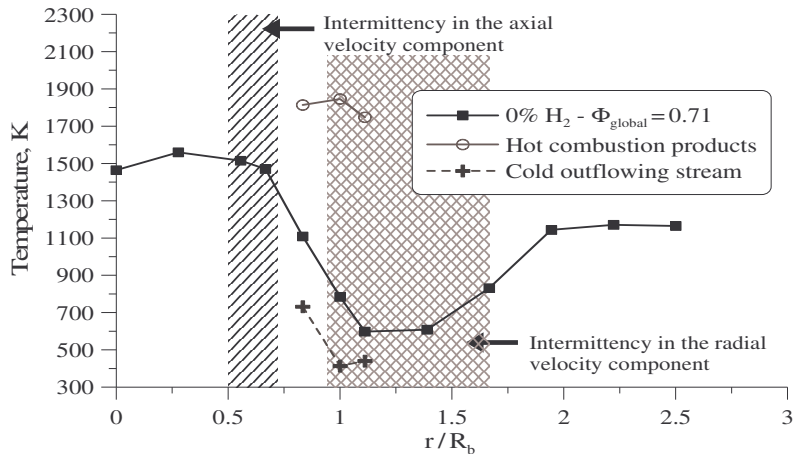


Fig. 8 Average and local temperature profiles: 0% hydrogen flame

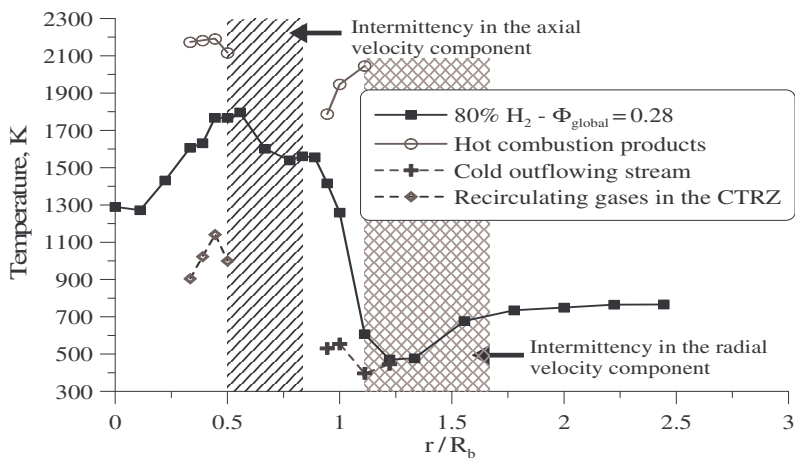


Fig. 9 Average and local temperature profiles: 80% hydrogen flame

4 Conclusions

In the present work combustion characteristics of methane-hydrogen-air reacting mixtures were investigated inside a non-premixed swirl burner by laser diagnostics. The combined use of PIV, LDV and Rayleigh scattering techniques was suitable in order to characterize mixing processes inside the flame. Indeed temperature and velocity measurements clearly showed that the region located between the outer boundary of the CTRZ and the inner boundary of the CRZ was characterized by the presence of two shear layers generated by the interaction between the reverse flow, carrying hot combustion products, the cold out flowing reactants stream and hot recirculating gases in the CRZ. Finally, temperature and velocity PDFs analysis revealed that even if the global

flow field was characterized by an intense mixing process, generated by the swirl motion, local non-uniformities were still present and had a considerable impact on pollutants emissions.

References

- Choudhuri AR, Gollahalli SR (2003) Characteristics of Hydrogen-Hydrocarbon Composite Fuel Turbulent Jet Flames. *International Journal of Hydrogen Energy* 28(4):445-454
- Coghe A, Solero G, Scribano G (2004) Recirculation Phenomena in a Natural Gas Swirl Combustor. *Experimental Thermal and Fluid Science* 28:709-714
- Cozzi F, Coghe A (2006) Behavior of hydrogen-enriched non-premixed swirled natural gas flames. *International Journal of Hydrogen Energy* 31(6):669-677
- Drake MC, Pitz RW, Lapp M (1986) Laser Measurements on Nonpremixed H₂-Air Flames for Assessment of Turbulent Combustion Models. *AIAA J.* 24:905-917
- Gupta AK, Lilley DG, Syred N (1984) *Swirl Flows*. Tunbridge Wells, Abacus Press
- Halthore RN, Gouldin FC (1986) Laser Scattering Measurements for Gas Densities in a Swirling Flow Combustor. *AIAA J.* 24:1129-1136
- Kruppa B, Strube G (1994) Light Scattering. In: *Optical Measurements: Techniques and Applications* (ed. Mayinger F). pp. 159-177, Springer-Verlag
- Jackson GS, Sai R, Plaia JM, Boggs CM, Kiger KT (2003) Influence of H₂ on the Response of Lean Premixed CH₄ Flames to High Strained Flows. *Comb. and Flame* 132:503-511
- Ji J, Gore J (2002) Flow Structure in Lean Premixed Swirling Combustion. 29th Symp (Int) on Combustion. The Combustion Institute, pp. 861-867
- Meier W, Duan XR, Weigand P (2006) Investigation of Swirl Flames in Gas Turbine Model Combustor: Turbulence-Chemistry Interactions. *Combustion and Flame* 144:225-236
- Nabizadeh H, Mayinger F (1999) Viscosity of Binary Mixtures of Hydrogen and Natural Gas (Hythane) in the Gaseous Phase. 15th European Conference on Thermophysical Properties, Würzburg, Germany, pp. 19-30
- Namer I, Schefer RW (1985) Error Estimates for Rayleigh Scattering Density and Temperature Measurements in Premixed Flames. *Experiments in Fluids* 3:1-9
- Olivani A, Cozzi F, Solero G, Coghe A (2005) Analysis of the Environmental Impact of a Swirl Burner: Hydrogen and Natural Gas Mixture Feeding. 28th Meeting of the Italian Section of The Combustion Institute, Napoli, Italy
- Qi S, Gupta AK, Lewis MJ (1997) Effect of Swirl on Combustion Characteristics in Premixed Flames. *Proc. of the ASME Int. Gas Turbine and Aeroengine Congress*, Orlando, FL
- Schefer RW (2003) Hydrogen Enrichment for Improved Lean Flame Stability. *International Journal of Hydrogen Energy* 28:1131-1141
- Schefer RW, Wicksall DM, Agrawal AK (2002) Combustion of Hydrogen-Enriched Methane in a Lean Premixed Swirl-Stabilized Burner. 29th Symp (Int) on Combustion. The Combustion Institute, pp. 843-851
- Tangirala V, Driscoll JF (1988) Temperature within Non-premixed Flames: Effects of Rapid Mixing Due to Swirl. *Combustion Science and Technology* 60:143-162
- Vanoverberghe K, Van Den Bulck E, Tummers M (2004) Flow Structure of Lifted Swirling Jet Flames. *Flow Turb. and Comb.* 73: 25-47
- Weigand P, Meier W, Duan XR, Stricker W, Aigner M (2006) Investigation of Swirl Flames in Gas Turbine Model Combustor: Flow Field, Structures, Temperature and Species Distributions. *Combustion and Flame* 144:205-224